Journal of Power Sources 336 (2016) 419–426

Contents lists available at ScienceDirect

Journal of Power Sources

journal homepage: www.elsevier.com/locate/jpowsour

# Electrochemical performance of a superporous activated carbon in ionic liquid-based electrolytes

Sarai Leyva-García [a], Dolores Lozano-Castelló [a], Emilia Morallón [b], Thomas Vogl [c], Christoph Schütter [d], Stefano Passerini [c], Andrea Balducci [d], Diego Cazorla-Amorós [a, *]

[a] Departamento de Química Inorgánica e Instituto Universitario de Materiales, Universidad de Alicante, Apdo. 99, Alicante, Spain
[b] Departamento de Química Física e Instituto Universitario de Materiales, Universidad de Alicante, Apdo. 99, Alicante, Spain
[c] Helmholtz Institute Ulm and Karlsruhe Institute of Technology (KIT), Helmholtzstraße 11, 89081 Ulm, Germany
[d] Institute for Technical Chemistry and Environmental Chemistry and Center for Energy and Environmental Chemistry (CEEC), Philosophenweg 7a, 07743 Jena, Germany

## HIGHLIGHTS

- Tailored porosity of ANK3 makes possible to achieve excellent electrochemical behaviour.
- Capacitance values of ANK3 improves those for other ACs in non-aqueous electrolytes.
- ANK3 is an excellent candidate as electrode for non-aqueous electrolytes-based EDLC.

## GRAPHICAL ABSTRACT

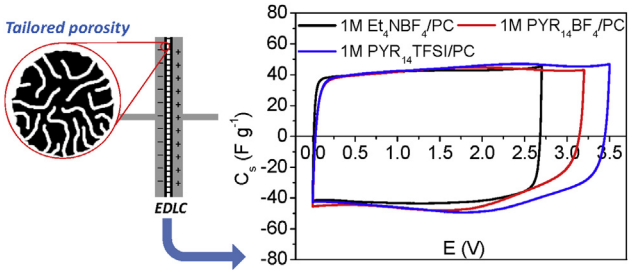


## ARTICLE INFO

*Article history:*
Received 29 July 2016
Received in revised form
26 September 2016
Accepted 3 November 2016
Available online 10 November 2016

*Keywords:*
Superporous activated carbon
Ionic liquid
Supercapacitor
Capacitance

## ABSTRACT

The electrochemical behaviour of a superporous activated carbon (named as ANK3) with a tailored porosity (high apparent specific surface area and a high volume of micropores with an average pore size of around 1.4 nm) is analysed in different non-aqueous electrolytes. ANK3 shows very high capacitance (higher than 160 F $g^{-1}$) values in solvent-free electrolytes at different temperatures (20, 40 and 60 °C) as well as in 1 M $Et_4N$ $BF_4$/PC, 1 M $PYR_{14}$ $BF_4$/PC and 1 M $PYR_{14}$ TFSI/PC. The tailored porosity of the ANK3, makes possible to obtain very high capacitance values, making this superporous activated carbon a promising candidate to be used as electrode for electrochemical capacitors using both organic and ionic liquid electrolytes. It is also confirmed that several parameters, such as the ion/pore size ratio, the ion shape, the ion solvation and the conductivity and viscosity of the electrolyte have a strong influence on the electrochemical behaviour of the ANK3.



## 1. Introduction

Electrochemical double-layer capacitors (EDLCs), or supercapacitors, based on the formation of the electric double-layer (EDL) in the interphase electrode-electrolyte and the quick faradic charge transfer reactions between the electrolyte and the electrode (i.e. pseudocapacitance), are currently considered one of

* Corresponding author. Departamento de Química Inorgánica e Instituto Universitario de Materiales, University of Alicante, P.O. Box 99, San Vicente del Raspeig, E-03080, Alicante, Spain.
*E-mail address:* cazorla@ua.es (D. Cazorla-Amorós).

http://dx.doi.org/10.1016/j.jpowsour.2016.11.010
0378-7753/

the most promising electrochemical energy storage devices [1,2]. Presently the main goal of the studies dedicated to these devices is to design high energy (>10 Wh $kg^{-1}$) devices displaying the high power of state-of-the art EDLCs [3].

The energy density of an EDLC is described by equation (1),

$$E = \frac{1}{2} \cdot C \cdot V^2 \quad (1)$$

where $E$ is the energy, $C$ is the capacitance and $V$ is the operating voltage.

Thus the increase of both the capacitance and the operating voltage are the two strategies to improve the energy stored.

Porous carbon materials and, in particular, activated carbons (ACs) are one of the most suitable electrode materials for EDLCs because of their low-cost, versatility of both structure/texture and surface chemistry, good conductivity and high cycling life [4,5]. Regarding the carbon material properties, the surface chemistry plays a key role because it can affect the wettability of the electrolyte and contribute to the pseudocapacitance, but also it has a strong influence on the stability of the capacitor upon cycling [6,7]. Furthermore, due to the EDL mechanisms in supercapacitors based on carbon electrodes, porous structure and pore size distribution are key parameters to improve the capacitance of the electrodes [1,5,8]. It is now well known that pores with diameters comparable to the effective ion size are optimal for high specific capacitance [9]; however, extremely narrow pores may present sieving effect and, in consequence, they do not contribute to the charge stored [2,6,10–12].

Aqueous solution, organic solution and ionic liquids (ILs) are currently used as electrolytes for supercapacitors. Aqueous electrolytes display high capacitance values but a relatively low operating voltage of around 1.0 V, though an operating voltage up to 1.8 V can be reached using neutral aqueous solution [4,13]. Organic electrolytes, typically based on quaternary ammonium salt dissolved in an organic solvent, usually propylene carbonate (PC) or acetonitrile (ACN), provide a stability window in the range of 2.5–2.7 V [10,14] that display a higher specific energy than aqueous systems (even though they show less ionic conductivity and capacitance values). However, ILs are currently considered one of the most interesting electrolytes because they show non-flammability and negligible vapor pressure (and thus, high safety), high thermal stability and a wide electrochemical stability window that provides operative voltage higher than 3 V [15]. The main drawback of ILs is the high viscosity and low conductivity compared to electrolytes based on PC and ACN that might affect the capacitance values displayed by electrode materials [16]. To overcome this limitation, mixtures of ILs and organic solvents have been proposed and they are now considered as a convenient strategy to merge the favorable properties of these two classes of electrolytes.

Supercapacitors and batteries are mainly used for applications where the electronic systems have to operate at a wide range of temperatures (i.e. between -30 °C and +60 °C) [17] thus several works studying the electrochemical behaviour of these devices using IL-based electrolytes at different temperatures can be found in the literature [8,18,19].

In the past years the large majority of the investigated ACs have been developed for use in either aqueous or conventional organic electrolytes for EDLCs. Only few studies have been dedicated to the development of ACs tailored for alternative electrolytes, e.g. IL-based one. For this reason, this latter investigation appears of importance to take fully advantage of the favorable features of IL-based electrolytes.

The main objective of the present work is to characterize an AC with tailored porosity (high apparent specific surface area and a high volume of micropores with an average pore size of around 1.4 nm) for innovative electrolytes (solvent-free and solvent-based) for high voltage EDLCs. The influence of the ion/pore size ratio and the electrolyte characteristics (i.e. viscosity and conductivity) on the electrochemical behaviour of the investigated AC was studied in three PC-based electrolytes (1 M tetraethylammonium tetrafluoroborate in PC (1 M $Et_4N$ $BF_4$/PC), 1 M 1-butyl-1-methylpyrrolidinium tetrafluoroborate in PC (1 M $PYR_{14}$ $BF_4$/PC) and 1 M 1-butyl-1-methylpyrrolidinium bis-(trifluoromethylsulfonyl)imide in PC (1 M $PYR_{14}$ TFSI/PC)), and in the IL $PYR_{14}$ TFSI at different temperatures (20, 40 and 60 °C).

## 2. Experimental

### 2.1. Synthesis of the activated carbon

The superporous AC (named as ANK3) was obtained by KOH activation of anthracite, following the procedure described elsewhere [20]. Synthesis conditions were selected in order to obtain both high apparent specific surface area and high micropore volume. Briefly, the activating agent carbon precursor mixture (ratio 3:1) was heated up to 750 °C during 2 h (ramp of 5 °C $min^{-1}$). Afterwards, ANK3 was washed several times with a 5 M HCl solution and with distilled water until free of chloride ions. Finally, the sample was dried at 110 °C for 12 h.

### 2.2. Porous texture characterization

The porous texture of the ANK3 was determined by physical adsorption ($N_2$ at -196 °C and $CO_2$ at 0 °C) using an Autosorb-6 equipment (Quantachrome) after samples out-gassing at 250 °C under vacuum for 4 h. The total micropore volume (i.e. pore size smaller than 2 nm) was calculated from the application of the Dubinin–Radushkevich (DR) equation to the $N_2$ adsorption data at -196 °C ($0.005 < P\,P_0^{-1} < 0.17$). The narrow micropore volume (i.e. pore size smaller than around 1 nm) was estimated from $CO_2$ adsorption at 0 °C using the DR equation and applied to the higher relative pressure region [21–23]. The apparent specific surface area was calculated by applying the Brunauer–Emmett–Teller theory ($S_{BET}$). This method is commonly used to calculate the apparent specific surface area of the materials despite BET analysis could be inadequate for some microporous materials [24]. Thus, specific surface area was also calculated by applying non-local density functional theory ($S_{NLDFT}$) to the $N_2$ adsorption data. Pore size distribution (PSD) was calculated by applying the NLDFT model to the $N_2$ adsorption data [25,26] as applied by the Solution of Adsorption Integral Equation Using Splines Software (SAIEUS, available online at http://www.nldft.com/), using Heterogeneous Surface Model.

### 2.3. Surface chemistry characterization

Temperature programmed desorption (TPD) was performed in a DSC-TGA equipment (TA Instruments, SDT 2960 Simultaneous) coupled to a mass spectrometer (Thermostar, Balzers, GSD 300 T3), to characterize the surface chemistry of the ANK3. In this experiment, approximately 10 mg of the sample were heated up to 950 °C (heating rate 20 °C $min^{-1}$) under a helium flow rate of 100 ml $min^{-1}$.

### 2.4. Electrolytes preparation

Before preparing the electrolytes the conductive salts were pretreated. The IL $PYR_{14}$ TFSI (IoLiTec, 99.5%) was dried over molecular sieve (3 Å) until the water content was below 20 ppm. $Et_4N$ $BF_4$ (Sigma-Aldrich ≥ 99%) was also dried under vacuum. $PYR_{14}$ $BF_4$

(IoLiTec, 99%) was purified as described elsewhere [27]. PC (Sigma-Aldrich 99.7%) was used as organic solvent. Both the storing of the salts, IL and PC as well as the preparation of the electrolytes were done in a dry room (relative humidity < 0.2%).

### 2.5. Electrochemical characterization

ANK3 electrodes were composed of 90 wt % of ANK3 powder as active material, 5 wt % of carbon black (SUPER C65) as conductivity promoter and 5 wt % of sodium carboxymethylcellulose as binder (CMC from Walocel CRT 2000 GA). First of all, 0.025 g of CMC was dissolved in 1.6 mL of ultrapure water by magnetic stirring for 1 h. Afterwards, a mixture composed of 0.450 g of ANK3 and 0.025 g of carbon black was added and it was kept 30 min stirring at 5000 rpm using a rotary disk (Dremel 4000, Dremel Europe). Subsequently, the homogenous slurry was casted on aluminium foil (30 μm, purity > 99.9%, etched by immersion in 5 wt % KOH at 60 °C for 60 s) by using a laboratory scale doctor blade coater. The casted electrodes were left drying overnight at room temperature. After drying, electrodes with a diameter of 12 mm were cut from the coated sheets. The ANK3 electrodes prepared showed thickness values between 150 and 300 μm and average mass values between 1.5 and 6.0 mg.

Free standing electrodes (named as NORIT) with mass loadings over 40 mg were prepared using a different binder (polytetrafluoroethylene, PTFE, 60 wt % dispersion in $H_2O$, Sigma–Aldrich) and a microporous commercial AC (NORIT DLC Super 30, with a BET surface area of 1618 $m^2\ g^{-1}$) as an active material, with a final ratio of 85:10:5 (AC:carbon black:PTFE). The PTFE aqueous dispersion, the AC and the carbon black were dispersed in an excess amount of EtOH and stirred until viscous slurry was obtained. Then, the slurry was rolled and electrodes of 12 mm diameter were cut and left dried at 80 °C overnight.

Both the ANK3 and NORIT electrodes were dried under vacuum at 120 °C overnight before using them.

Electrochemical tests were carried out using the Swagelok®-type configuration. The cells were assembled in an argon-filled glove box with oxygen and water contents <1 ppm. Whatman GF/D glass microfiber filter of 675 μm in thickness and 13 mm in diameter was used as separator. Before assembly the cell, the separator was drenched with 140 μL of electrolyte and carbon electrodes were soaked under vacuum during 5 min. All the electrochemical tests were performed using a VMP multichannel potentiostatic-galvanostatic system (Biologic Science Instruments). Electrochemical cells were placed in an oven to keep a constant temperature during the measurements.

Electrochemical characterization of ANK3 in different electrolytes and at different temperatures was performed by using a standard three-electrode configuration. NORIT electrodes were used as counter electrode so as not to limit the capacitive response of the working electrode, while Ag wire was used as quasi-reference electrode. For EDLC characterization, asymmetric (in mass) supercapacitors were assembled to maximise the specific energy [28,29], ANK3 electrodes were used both as positive and negative electrode.

Prior to electrochemical characterization, the assembled cells remained 24 h at the selected temperature and, afterwards, 30 scans at 5 mV $s^{-1}$ were performed to ensure that the electrode was properly wetted by the electrolyte.

Cyclic voltammograms (CVs) were obtained at 1 mV $s^{-1}$ using three-electrode configuration. CVs were recorded at different potential ranges by broadening 0.10 V the potential limit of every cycle with respect to the previous one. Regarding cyclic voltammetry characterization of the EDLC, CVs were carried out at different scan rates ranging from 1 to 200 mV $s^{-1}$ at a given potential window. In both experiments, three scans were recorded at each condition.

From the 3rd steady-state CVs capacitance values were calculated using equations (2)–(4):

$$C_s = \frac{\frac{Q}{2}}{\Delta E \cdot m} \tag{2}$$

where $C_s$ is the specific capacitance (F $g^{-1}$), Q is the total electrical charge obtained by integration of the CV (C), ΔE is the potential window (V) and m is the ANK3 active mass of the electrode (g).

$$C_{n,BET} = \frac{C_s}{S_{BET}} \cdot 1000 \tag{3}$$

where $C_{n,BET}$ is the normalized capacitance (mF $m^{-2}$) and $S_{BET}$ is the apparent specific surface area of ANK3 calculated by applying the BET ($m^2\ g^{-1}$).

$$C_{n,NLDFT} = \frac{C_s}{S_{NLDFT}} \cdot 1000 \tag{4}$$

where $C_{n,NLDFT}$ is the normalized capacitance (mF $m^{-2}$) and $S_{NLDFT}$ is the specific surface area of ANK3 calculated by applying the NLDFT ($m^2\ g^{-1}$).

## 3. Results and discussion

### 3.1. Porous texture and surface chemistry characterization

Figs. 1 and 2 show the $N_2$ adsorption isotherm and PSD respectively. The $N_2$ isotherm is of type I, according to the IUPAC classification [30], typical of microporous materials. The PSD plot shows that ANK3 is an essentially microporous material with a wide micropore size distribution and a mean pore size of around 1.4 nm.

Table 1 shows the porous texture and surface chemistry characterization of ANK3. It can be seen that the ANK3 shows high apparent specific surface area and large micropore volume. $V_{DR}$ ($CO_2$) also indicates that the AC presents narrow microporosity (i.e., micropores less than 1 nm, approximately).

Surface oxygen groups of carbon materials decompose upon heating producing CO and $CO_2$ at different temperatures which can be followed by the TPD experiments [31,32]. Evolution of CO occurs at high temperatures as consequence of the decomposition of basic or neutral groups such as phenols, ethers, carbonyls and quinones.

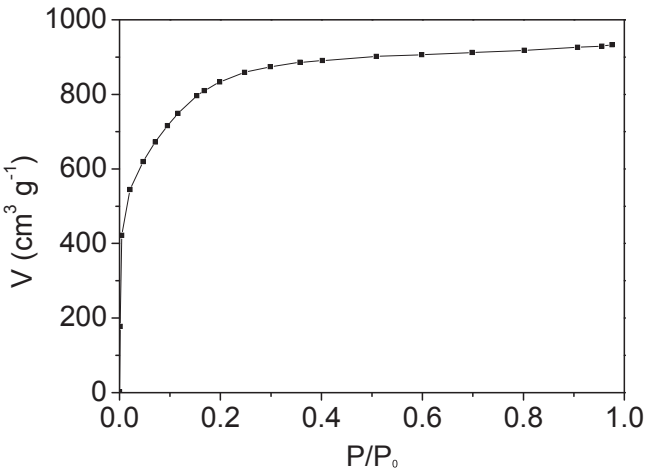


**Fig. 1.** $N_2$ adsorption isotherm at 77 K of ANK3.

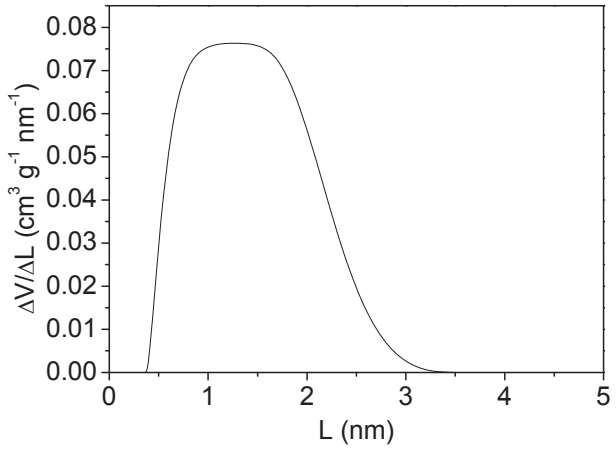


**Fig. 2.** PSD of ANK3 obtained from the $N_2$ isotherm at 77 K by applying NLDFT method.

$CO_2$ evolves generally at lower temperatures and it is mainly due to the decomposition of carboxylic groups and lactones. Decomposition of anhydride groups produces CO and $CO_2$. From the TPD profiles (not shown here), the amount of CO and $CO_2$ evolved groups were estimated and included in Table 1.

### 3.2. Electrochemical characterization in three-electrode configuration

Steady-state CVs performed in three-electrode configuration in the electrolytes 1 M $Et_4N$ $BF_4$/PC, 1 M $PYR_{14}$ $BF_4$/PC and 1 M $PYR_{14}$ TFSI/PC, at 20 °C, are shown in Fig. 3.

First of all, it should be remarked that for both potential windows, for the three electrolytes, black CVs show a quasi-rectangular shape, typical of an essentially capacitive process associated with the formation of the EDL.

Concerning the more positive potential window, red and blue CVs show an anodic current at high potential values, for the three electrolytes. It should be noted that this anodic current is higher for the experiments performed in 1 M $Et_4N$ $BF_4$/PC medium. The corresponding cathodic peak is observed at around 0.80 V both in 1 M $Et_4N$ $BF_4$/PC and 1 M $PYR_{14}$ TFSI/PC and at approximately 1.00 V in 1 M $PYR_{14}$ $BF_4$/PC. As it will be discussed below, several parameters influence the electrochemical behaviour of the ANK3 in the three electrolytes, justifying the potential values registered for the cathodic process even though both anions and cations of the 1 M $Et_4N$ $BF_4$/PC and 1 M $PYR_{14}$ TFSI/PC electrolytes are different while, 1 M $PYR_{14}$ $BF_4$/PC presents the same $BF_4^-$ anion that 1 M $Et_4N$ $BF_4$/PC.

Regarding the less positive potential window, it seems that reduction processes take place at negative potential values (see red, blue, green and purple CVs); in fact, a cathodic current is recorded starting from −1.20, −1.70 and −2.00 V to less positive potential in 1 M $Et_4N$ $BF_4$/PC, 1 M $PYR_{14}$ $BF_4$/PC and 1 M $PYR_{14}$ TFSI/PC media, respectively. The corresponding anodic peak is observed during the positive scan at around -0.61, -0.30 and -0.44 V for 1 M $Et_4N$ $BF_4$/PC, 1 M $PYR_{14}$ $BF_4$/PC and 1 M $PYR_{14}$ TFSI/PC, respectively (see red, blue, green and purple CVs). It should be noted that the anodic peak is shifted to more positive potentials, and its intensity increases when

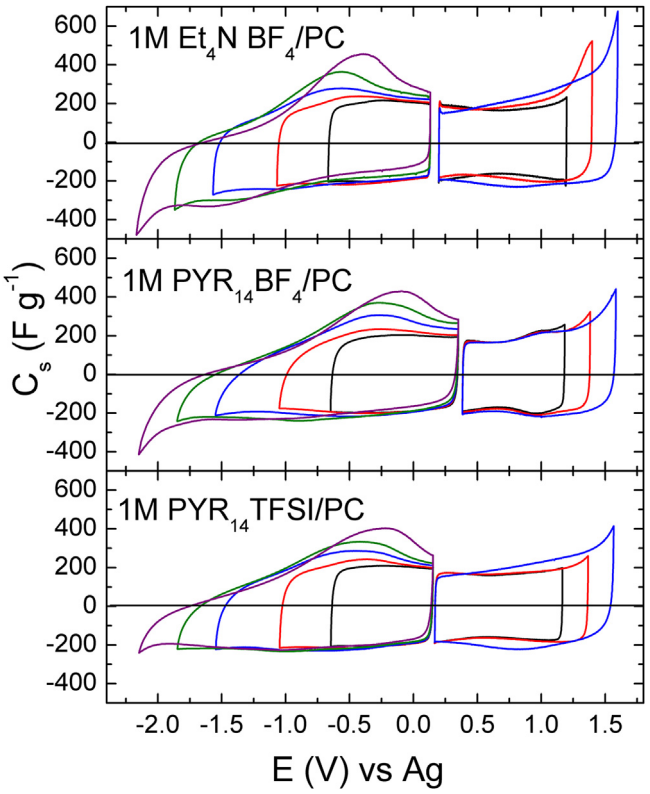


**Fig. 3.** CVs in three-electrode configuration in: 1 M $Et_4N$ $BF_4$/PC, 1 M $PYR_{14}$ $BF_4$/PC and 1 M $PYR_{14}$ TFSI/PC. 1 mV $s^{-1}$ scan rate. 20 °C.

increasing the negative potential limit down to -2.10 V (see purple CV), for the three electrolytes. These redox processes may be related both to faradic charge transfer reactions (i.e. pseudocapacitance), due to the presence of surface oxygen groups in the ANK3 [6,16], and/or to decomposition of PC [8,33]. It has been shown that the aging rate of symmetric EDLC is dominated by the aging of the negative electrode, in PC-based electrolytes [34]. It is known that the electrochemical decomposition of PC can be promoted by the presence of the surface functionalities, that is to say, the solvent can react with functional groups on the ACs. Furthermore inorganic impurities of ACs that could remain after chemical activation may facilitate the irreversible decomposition of PC (in this case, ANK3 shows a residual potassium content below 1 wt % [20]). The degradation of the PC might produce a blockage of the porosity [8,33]; it has been suggested that propene and $H_2$ come from PC reduction and $CO_2$ is produced by PC oxidation [33].

It should be noted that, when broadening the potential window, both the anodic and cathodic currents registered seems to indicate that the operative potential window increases as follows: 1 M $Et_4N$ $BF_4$/PC < 1 M $PYR_{14}$ $BF_4$/PC < 1 M $PYR_{14}$ TFSI/PC, that is in agreement with the literature [10,14,16].

From the CVs performed between the open circuit potential ($E_{oc}$) and −0.65 V and from $E_{oc}$ to 1.20 V (black curves), the capacitance values displayed by cations and anions of the electrolytes were calculated (see Table 2). As shown in the table, the ANK3-based electrodes are displaying specific capacitance values

**Table 1**
Porous texture and surface chemistry characterization results of ANK3.

| $S_{BET}$ ($m^2$ $g^{-1}$) | $S_{NLDFT}$ ($m^2$ $g^{-1}$) | $V_{DR}$ ($N_2$) ($cm^3$ $g^{-1}$) | $V_{DR}$ ($CO_2$) ($cm^3$ $g^{-1}$) | μmolCO $g^{-1}$ | μmol$CO_2$ $g^{-1}$ | μmolO $g^{-1}$ |
|---|---|---|---|---|---|---|
| 3165 | 2130 | 1.17 | 0.81 | 2160 | 590 | 3340 |

which are exceeding 180 F $g^{-1}$. To the best of our knowledge, these values are among the highest so far reported for AC-based electrodes in non-conventional electrolyte. The $C_s$ for $TFSI^-$ is slightly lower than that shown by $BF_4^-$. The ion size of $BF_4^-$ has been estimated to be 0.46 nm [10] (considering that it has a spherical shape), while ion dimensions of $TFSI^-$ are, approximately, 0.79 nm and 0.29 nm [9]. Both shape and ion size with respect to the pore size, influence the adsorption in the micropores. If only one layer of ions was adsorbed in the pores, the smaller the distance between the pore wall and the centre of the ion, the higher the capacitance, what could provide higher specific capacitance for $TFSI^-$. However, when increasing the pore size, if a second layer could be accommodated, the capacitance would increase [35]. In this case, the activated carbon used has a wide micropore size distribution and an average pore size of 1.4 nm that can accommodate at least two layers of spherical $BF_4^-$ anions with a more efficient packing than $TFSI^-$. Other parameters should be taken into account such as ion solvation, conductivity and viscosity. It has been shown that for the entrance of the ions into the pores they have to be at least partially desolvated [2,9,35,36]. Also the lower conductivity and higher viscosity of 1 M $PYR_{14}$ TFSI/PC compared to both 1 M $Et_4N$ $BF_4$/PC and 1 M $PYR_{14}$ $BF_4$/PC (see Table 3) explains the lower $C_s$ of $TFSI^-$ compared to that displayed by $BF_4^-$. Even though viscosity and conductivity of 1 M $Et_4N$ $BF_4$/PC and 1 M $PYR_{14}$ $BF_4$/PC are quite similar, the fact that both ions, and not only the counterions (with the opposite charge as that of the charged electrode) are involved in the EDL formation [12] may justify the different $C_s$ values calculated for $BF_4^-$ in these two electrolytes.

The $C_s$ of $Et_4N^+$ (calculated from 1 M $Et_4N$ $BF_4$/PC) is slightly higher than that shown by $PYR_{14}^+$ (calculated from 1 M $PYR_{14}$ $BF_4$/PC) but almost equal to that shown by $PYR_{14}^+$ (calculated from 1 M $PYR_{14}$ TFSI/PC). In this case, the diameter of $Et_4N^+$ is 0.69 nm [10] (considering that it has a spherical shape), while the dimensions of $PYR_{14}^+$, which has been estimated using the Avogadro software, are around 1.10 nm and 0.65 nm (see Fig. 4). If $PYR_{14}^+$ is adsorbed with the longest dimension perpendicular to the pore wall, both $Et_4N^+$ and $PYR_{14}^+$ would have similar distance between the pore wall and the centre of the ion and, then, similar $C_s$. Since the activated carbon used has a wide micropore size distribution with an average pore size of 1.4 nm, the pores are wide enough to accommodate the larger cations giving similar capacitances.

It is well known, that not only the apparent specific surface area but also PSD and surface chemistry affects to the capacitance displayed by carbon materials both in aqueous and non-aqueous electrolytes [6,7,9,12,37]. The ratio between the pore width and the ion size is a key parameter that strongly affects the electrochemical behaviour. It has been demonstrated that pore size very close to the ion size leads to the maximum capacitance [9], however ion access to very narrow micropores (i.e. non-accessible pores) may be hindered (thus showing sieving effect) [6,12].

In this study, the porosity of the AC has been tailored in order to obtain a high apparent specific surface area and a high volume of micropores with an average pore size of around 1.4 nm. This tailored porosity makes possible to reach very high $C_s$ values, in the three electrolytes, since this material provides wider micropores for an efficient adsorption and accommodation of ions for the different ion sizes studied in this work. For this reason, these results improve those found in the literature for other ACs in non-aqueous electrolytes (using both ACN and PC as solvent) [10,38–40]. $C_{n,NLDFT}$ values are comparable to that showed for ACs that do not present sieving effect [10], thus suggesting that most of the porosity is fully accessible to the ions of the electrolytes, because the pore size (of around 1.4 nm) is higher than the ion size of the electrolytes used.

**Table 2**
Capacitance values calculated for the ions of the three electrolytes (1 M $Et_4N$ $BF_4$/PC, 1 M $PYR_{14}$ $BF_4$/PC and 1 M $PYR_{14}$ TFSI/PC) in three-electrode configuration.

| | $C_s$ (F $g^{-1}$) | | $C_{n,BET}$ (mF $m^{-2}$) | | $C_{n,NLDFT}$ (mF $m^{-2}$) | |
|---|---|---|---|---|---|---|
| | Anion | Cation | Anion | Cation | Anion | Cation |
| 1 M $Et_4N$ $BF_4$/PC | 179 | 197 | 57 | 62 | 84 | 93 |
| 1 M $PYR_{14}$ $BF_4$/PC | 187 | 185 | 59 | 58 | 88 | 87 |
| 1 M $PYR_{14}$ TFSI/PC | 168 | 195 | 53 | 62 | 79 | 92 |

**Table 3**
Viscosity and conductivity of the electrolytes at 20 °C [10].

| | Viscosity (mPa s) | Conductivity (mS $cm^{-1}$) |
|---|---|---|
| 1 M $Et_4N$ $BF_4$/PC | 4.0 | 10.7 |
| 1 M $PYR_{14}$ $BF_4$/PC | 4.2 | 9.8 |
| 1 M $PYR_{14}$ TFSI/PC | 5.1 | 7.3 |

CVs obtained for the pure IL $PYR_{14}$ TFSI at three different temperatures (20, 40 and 60 °C) are shown in Fig. 5. CVs performed in the pure $PYR_{14}$ TFSI at 20 °C show distorted shape compared to that recorded at 40 and 60 °C, that exhibit a quasi-rectangular shape typical of an essentially capacitive process associated with the formation of the EDL. The increase of conductivity and decrease of viscosity when increasing temperature [15,41,42] may explain these results. Furthermore, $PYR_{14}^+$ cation seems to present diffusional problems at 20 °C, presumably due both to: (i) the higher size of $PYR_{14}^+$ (1.10 and 0.65 nm, see Fig. 4) compared to $TFSI^-$ (0.79 and 0.29 nm [9]) with respect to the mean pore size of ANK3 (around 1.4 nm) and (ii) the characteristics of the electrolyte at this temperature (i.e. conductivity and viscosity) [16]. On the other hand, the comparison of CVs performed at 20 °C in the pure $PYR_{14}$ TFSI (Fig. 5) and in 1 M $PYR_{14}$ TFSI/PC (Fig. 3), reveals that conductivity increases and viscosity decreases when using the PC-containing electrolyte, as it has been previously seen [16,42]. Thus, it seems that electrochemical behaviour is affected not only by ion/pore size ratio and ion shape but also by viscosity and conductivity of the IL (that vary both by diluting the IL with organic solvents and by changing IL temperature) [43].

It should be noted that by increasing the potential limits (both positive and negative window) several redox peaks are observed for the three temperatures. At 20 °C, an anodic peak is observed at approximately 1.15 V and the corresponding cathodic peak is seen at around 0.95 V. These redox processes are observed at 1.00 V (anodic peak) and at 1.10 V (cathodic peak) for the CVs performed at 40 and 60 °C. Furthermore, three oxidation peaks are observed at around −0.22, −0.67 and −1.10 V for the CVs performed at 40 and 60 °C, when reaching potential limits down to −2.30 and −2.00 V, respectively. Even at 20 °C, a slight anodic peak is observed at −0.70 V after reaching the negative potential of −2.50 V. These redox peaks may be due both to faradic charge transfer reactions

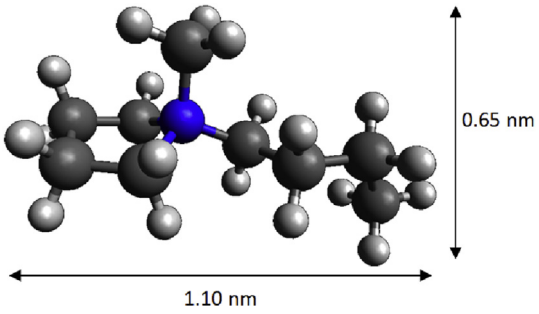


**Fig. 4.** Avogadro software model of the structure of $PYR_{14}^+$.

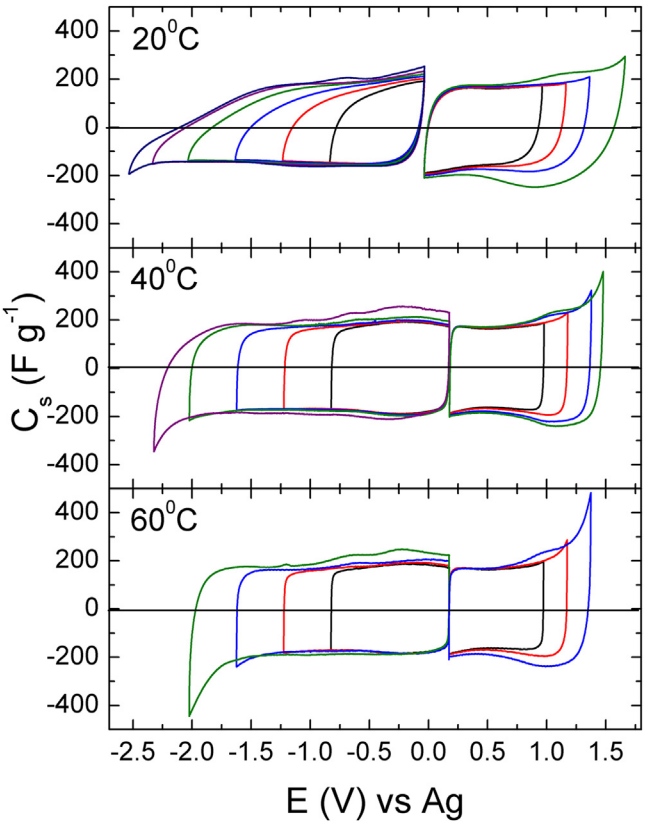


**Fig. 5.** CVs in three-electrode configuration in $PYR_{14}$ TFSI at 20, 40 and 60 °C. 1 mV $s^{-1}$ scan rate.

(i.e. pseudocapacitance), due to the presence of surface oxygen groups in the ANK3 [16], and/or to the degradation of the $PYR_{14}$ TFSI. It should be noted that the remarkable anodic peak observed at around -0.44 V for 1 M $PYR_{14}$ TFSI/PC (see Fig. 3) is not observed in the CVs performed in the pure $PYR_{14}$ TFSI, thus it is reasonable to suppose that decomposition of PC might take place at potentials lower than -1.20 V. Regarding potential stability window it seems to decrease when increasing temperature: a negative current is recorded starting from −2.30 V, −1.80 V and −1.50 V to more negative values and a positive current starts at, approximately, 1.50 V, 1.40 and 1.20 V for the CVs done at 20, 40 and 60 °C, respectively. These latter findings are in line with results already reported in the literature [2,43].

Table 4 shows capacitance values of $PYR_{14}^{+}$ and $TFSI^{-}$ calculated from the cyclic voltammograms performed between $E_{oc}$ and -0.82 V and between $E_{oc}$ and 0.97 V. Values obtained from the experiments performed at 40 and 60 °C are quite similar. Capacitance displayed by $PYR_{14}^{+}$ is slightly higher than that shown by the $TFSI^{-}$ anion; furthermore, the same trend was observed from 1 M $PYR_{14}$ TFSI/PC (see Table 2). However, this trend is not observed from the experiment done at 20 °C, where the higher size of $PYR_{14}^{+}$ cation leads to diffusional problems at this temperature.

**Table 4**
Capacitance values calculated for the ions of $PYR_{14}$ TFSI in three-electrode configuration.

| | $C_s$ (F $g^{-1}$) | | $C_{n,BET}$ (mF $m^{-2}$) | | $C_{n,NLDFT}$ (mF $m^{-2}$) | |
|---|---|---|---|---|---|---|
| | Anion | Cation | Anion | Cation | Anion | Cation |
| 20 °C | 149 | 132 | 47 | 42 | 70 | 62 |
| 40 °C | 167 | 176 | 53 | 56 | 78 | 83 |
| 60 °C | 167 | 174 | 53 | 55 | 78 | 82 |

It should be pointed out that the tailored porosity of ANK3 (high apparent specific surface area and a high volume of micropores with an average pore size of around 1.4 nm) allows to obtain very high $C_s$ values of around 170 F $g^{-1}$ in solvent-free electrolytes (showed by for both ions of $PYR_{14}$ TFSI at 40 and 60 °C). These values improve those found in the literature for high surface area carbon materials in $PYR_{14}$ TFSI [44,45] and in other IL [46] and for AC-based solid state supercapacitors [47] at 60 °C.

### 3.3. EDLC characterization

To complete the electrochemical characterization of the ANK3 in the PC-containing electrolytes studied, ANK3-based EDLCs were assembled and preliminary investigations were performed. The mass loadings of the active materials were balanced, according to the electrochemical stability limits and the $C_s$ values showed in each electrolyte, in order to avoid the premature aging of the cell and to enhance the electrochemical performance of the EDLCs [28,29,48,49]. The ratio of mass was calculated using equation (5):

$$\frac{m_+}{m_-} = \frac{C_{s-} \cdot \Delta E_-}{C_{s+} \cdot \Delta E_+} \quad (5)$$

where $m_+/m_-$ is the mass ratio between the positive and the negative electrode, $C_{s+}/C_{s-}$ is the respective $C_s$ and $\Delta E_+/\Delta E_-$ is the respective maximum operating potential window (calculated from three-electrode configuration experiments).

Three CVs were performed at 1, 2, 5, 20, 50, 100 and 200 mV $s^{-1}$ scan rates. Operative potential windows of 2.7, 3.2 and 3.5 V were reached for 1 M $Et_4N$ $BF_4$/PC, 1 M $PYR_{14}$ $BF_4$/PC and 1 M $PYR_{14}$ TFSI/PC, respectively. The 3rd steady CVs at 5 mV $s^{-1}$, for the three electrolytes, are presented in Fig. 6. The CVs show a quasi-rectangular shape, typical of an essentially capacitive process associated with the formation of the EDL. $C_s$ values, at each scan rate, were also calculated and they are shown in Fig. 7. It should be remarked the high $C_s$ value, of around 45 F $g^{-1}$ at 1 mV $s^{-1}$ scan rate, shown by ANK3 in the three electrolytes. Even though the comparison is not straightforward (because of the different electrochemical conditions), capacitance values obtained improve the results reported for different ACs in several non-aqueous electrolytes [8,10,16,27,34,50]. In 1 M $Et_4N$ $BF_4$/PC, the percentage value of retained capacitance at 200 mV $s^{-1}$ is 56%, which is higher than for

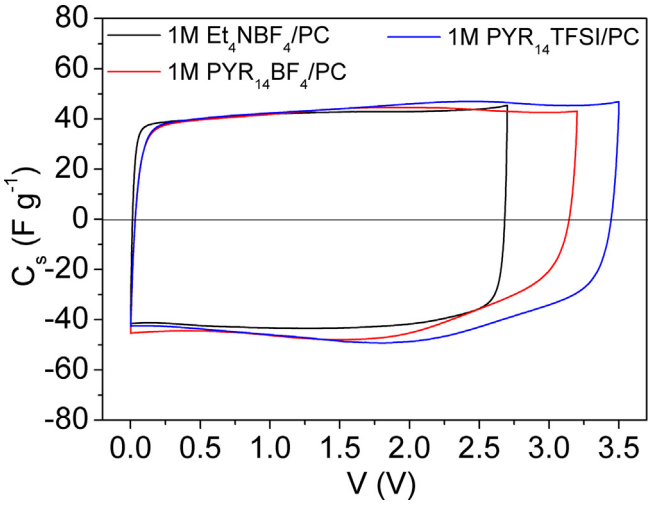


**Fig. 6.** CVs at 5 mV $s^{-1}$ in two-electrode configuration in: 1 M $Et_4N$ $BF_4$/PC, 1 M $PYR_{14}$ $BF_4$/PC and 1 M $PYR_{14}$ TFSI/PC. 20 °C.

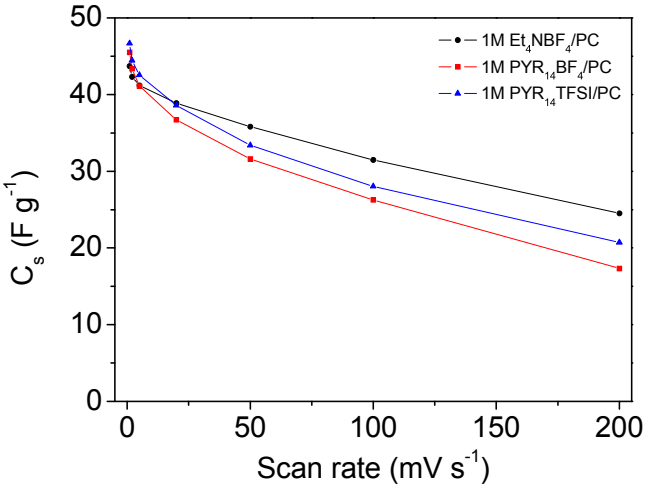


**Fig. 7.** $C_s$ values versus scan rate plot for: 1 M $Et_4N$ $BF_4$/PC, 1 M $PYR_{14}$ $BF_4$/PC and 1 M $PYR_{14}$ TFSI/PC.

the other two electrolytes. These results suggest that ion/pore size ratio, ion shape and viscosity and conductivity of the electrolyte have a strong influence on the electrochemical behaviour at higher scan rate. The excellent electrochemical behaviour shown by ANK3 (in terms of specific capacitance and retained capacitance) due to the tailored porosity of this AC makes it a promising candidate as electrode for EDLC both in organic and IL electrolytes.

## 4. Conclusions

Tailoring the porosity of the AC is one of the key to take fully advantages of the features of innovative electrolytes. We showed that using AC with high apparent specific surface area and high micropore volume with an average pore size of 1.4 nm it is possible to obtain very high capacitance values in the pure $PYR_{14}$ TFSI at three different temperatures (20, 40 and 60 °C) as well as in 1 M $Et_4N$ $BF_4$/PC, 1 M $PYR_{14}$ $BF_4$/PC and 1 M $PYR_{14}$ TFSI/PC at 20 °C, using a three-electrode configuration. Excellent electrochemical behaviour (in terms of capacitance and retained capacitance) was also shown by ANK3-based EDLC in 1 M $Et_4N$ $BF_4$/PC, 1 M $PYR_{14}$ $BF_4$/PC and 1 M $PYR_{14}$ TFSI/PC at 20 °C.

These results pointed out that the tailored porosity of the ANK3 makes it an excellent candidate to be used as electrode for the realization of high voltage, high energy EDLC containing non-conventional electrolytes.

Furthermore, it was confirmed that several parameters, such as the ion/pore size ratio, the ion shape, the ion solvation and the characteristics of the electrolyte (i.e. conductivity and viscosity) have a strong influence on the electrochemical behaviour shown by ANK3.

## Acknowledgment

The authors would like to thank the MINECO (MAT2013-42007-P and CTQ2015-66080-R MINECO/FEDER) and GV (PROMETEOII/2014/010). SLG thanks Spanish MECD for the thesis grant (personal reference number: AP-2012-5071) and DAAD foundation for the short-term grant (personal reference number: 91590114). AB, SP, TV and CS would like to thank you the gs5:Bundesministerium für Bildung und Forschung (BMBF) within the project IES (contract number 03EK3010) for the financial support.

## References

[1] F. Béguin, E. Raymundo-Piñero, E. Frackowiak, Electrical double-layer capacitors and pseudocapacitors, in: F. Béguin, E. Frackowiak (Eds.), Carbons for Electrochemical Energy Storage and Conversion Systems, CRC Press,Taylor & Francis Group, Boca Raton (USA), 2010, p. 329.
[2] F. Béguin, V. Presser, A. Balducci, E. Frackowiak, Carbons and electrolytes for advanced supercapacitors, Adv. Mater. 26 (2014) 2219–2251.
[3] J.R. Miller, P. Simon, Materials science - electrochemical capacitors for energy management, Science 321 (2008) 651–652.
[4] E. Frackowiak, F. Béguin, Carbon materials for the electrochemical storage of energy in capacitors, Carbon 39 (2001) 937–950.
[5] M.J. Bleda-Martínez, D. Lozano-Castelló, D. Cazorla-Amorós, E. Morallón, Kinetics of double-layer formation: influence of porous structure and pore size distribution, Energ. Fuel 24 (2010) 3378–3384.
[6] D. Lozano-Castelló, D. Cazorla-Amorós, A. Linares-Solano, S. Shiraishi, H. Kurihara, A. Oya, Influence of pore structure and surface chemistry on electric double layer capacitance in non-aqueous electrolyte, Carbon 41 (2003) 1765–1775.
[7] M.J. Bleda-Martínez, D. Lozano-Castelló, E. Morallón, D. Cazorla-Amorós, A. Linares-Solano, Chemical and electrochemical characterization of porous carbon materials, Carbon 44 (2006) 2642–2651.
[8] D. Cazorla-Amorós, D. Lozano-Castelló, E. Morallón, M.J. Bleda-Martínez, A. Linares-Solano, S. Shiraishi, Measuring cycle efficiency and capacitance of chemically activated carbons in propylene carbonate, Carbon 48 (2010) 1451–1456.
[9] C. Largeot, C. Portet, J. Chmiola, P. Taberna, Y. Gogotsi, P. Simon, Relation between the ion size and pore size for an electric double-layer capacitor, J. Am. Chem. Soc. 130 (2008) 2730–2731.
[10] S. Pohlmann, R. Kuehnel, T.A. Centeno, A. Balducci, The influence of anion-cation combinations on the physicochemical properties of advanced electrolytes for supercapacitors and the capacitance of activated carbons, Chem. Electro. Chem. 1 (2014) 1301–1311.
[11] E. Frackowiak, Q. Abbas, F. Beguin, Carbon/carbon supercapacitors, J.Energy Chem. 22 (2013) 226–240.
[12] M. Lazzari, M. Mastragostino, A.G. Pandolfo, V. Ruiz, F. Soavi, Role of carbon porosity and ion size in the development of ionic liquid based supercapacitors, J. Electrochem. Soc. 158 (2011) A22–A25.
[13] M.P. Bichat, E. Raymundo-Piñero, F. Beguin, High voltage supercapacitor built with seaweed carbons in neutral aqueous electrolyte, Carbon 48 (2010) 4351–4361.
[14] A. Brandt, A. Balducci, Theoretical and practical energy limitations of organic and ionic liquid-based electrolytes for high voltage electrochemical double layer capacitors, J.Power Sources 250 (2014) 343–351.
[15] M. Galinski, A. Lewandowski, I. Stepniak, Ionic liquids as electrolytes, Electrochim. Acta 51 (2006) 5567–5580.
[16] S. Pohlmann, B. Lobato, T.A. Centeno, A. Balducci, The influence of pore size and surface area of activated carbons on the performance of ionic liquid based supercapacitors, Phys. Chem. Chem. Phys. 15 (2013) 17287–17294.
[17] P. Simon, Y. Gogotsi, Materials for electrochemical capacitors, Nat. Mater. 7 (2008) 845–854.
[18] P. Huang, D. Pech, R. Lin, J.K. McDonough, M. Brunet, P. Taberna, Y. Gogotsi, P. Simon, On-chip micro-supercapacitors for operation in a wide temperature range, Electrochem. Commun. 36 (2013) 53–56.
[19] Y. Kado, K. Imoto, Y. Soneda, N. Yoshizawa, Highly enhanced capacitance of MgO-templated mesoporous carbons in low temperature ionic liquids, J.Power Sources 271 (2014) 377–381.
[20] D. Lozano-Castelló, M.A. Lillo-Ródenas, D. Cazorla-Amorós, A. Linares-Solano, Preparation of activated carbons from Spanish anthracite: I. Activation by KOH, Carbon 39 (2001) 741–749.
[21] D. Lozano-Castelló, D. Cazorla-Amorós, A. Linares-Solano, Usefulness of CO2 adsorption at 273 K for the characterization of porous carbons, Carbon 42 (2004) 1233–1242.
[22] D. Cazorla-Amorós, J. Alcaniz-Monge, M. de la Casa-Lillo, A. Linares-Solano, $CO_2$ as an adsorptive to characterize carbon molecular sieves and activated carbons, Langmuir 14 (1998) 4589–4596.
[23] P. Ravikovitch, A. Vishnyakov, R. Russo, A. Neimark, Unified approach to pore size characterization of microporous carbonaceous materials from $N_2$, Ar, and $CO_2$ adsorption isotherms, Langmuir 16 (2000) 2311–2320.
[24] J. Rouquerol, P. Llewellyn, F. Rouquerol, Is the BET equation applicable to microporous adsorbents? Stud. Surf. Sci. Catal. 160 (2007) 49–56.
[25] D. Lozano-Castelló, F. Suárez-García, D. Cazorla-Amorós, Á. Linares-Solano, Porous texture of carbons, in: F. Beguin, E. Frackowiak (Eds.), Carbons for Electrochemical Energy Storage and Conversion Systems, CRC Press,Taylor & Francis Group, Boca Raton (USA), 2010, p. 115.
[26] J. Jagiello, J.P. Olivier, 2D-NLDFT adsorption models for carbon slit-shaped pores with surface energetical heterogeneity and geometrical corrugation, Carbon 55 (2013) 70–80.
[27] C. Schütter, C. Ramírez-Castro, M. Oljaca, S. Passerini, M. Winter, A. Balducci, Activated carbon, carbon blacks and graphene based nanoplatelets as active materials for electrochemical double layer capacitors: a comparative study, J. Electrochem. Soc. 162 (2015) A44–A51.
[28] G.A. Snook, G.J. Wilson, A.G. Pandolfo, Mathematical functions for optimisation of conducting polymer/activated carbon asymmetric supercapacitors,

J.Power Sources 186 (2009) 216–223.
[29] C. Peng, S. Zhang, X. Zhou, G.Z. Chen, Unequalisation of electrode capacitances for enhanced energy capacity in asymmetrical supercapacitors, Energy Environ. Sci. 3 (2010) 1499–1502.
[30] K.S.W. Sing, D.H. Everett, R.A.W. Haul, L. Moscou, R.A. Pierotti, J. Rouquerol, T. Siemieniewska, Reporting physisorption data for gas solid systems with special reference to the determination of surface-area and porosity, Pure Appl. Chem. 57 (4) (1985) 603–619.
[31] M.C. Román-Martínez, D. Cazorla-Amorós, A. Linares-Solano, TPD and TPR characterization of carbonaceous supports and Pt/C catalysts, Carbon 31 (1993) 895–902.
[32] J. Figueiredo, M. Pereira, M. Freitas, J. Orfao, Modification of the surface chemistry of activated carbons, Carbon 37 (1999) 1379–1389.
[33] M. Hahn, A. Würsig, R. Gallay, P. Novák, R. Kötz, Gas evolution in activated carbon/propylene carbonate based double-layer capacitors, Electrochem. Commun. 7 (2005) 925–930.
[34] P.W. Ruch, D. Cericola, A. Foelske, R. Koetz, A. Wokaun, A comparison of the aging of electrochemical double layer capacitors with acetonitrile and propylene carbonate-based electrolytes at elevated voltages, Electrochim. Acta 55 (2010) 2352–2357.
[35] M.V. Fedorov, A.A. Kornyshev, Ionic liquids at electrified interfaces, Chem. Rev. 114 (2014) 2978–3036.
[36] D. Jiang, Z. Jin, D. Henderson, J. Wu, Solvent effect on the pore-size dependence of an organic electrolyte supercapacitor, J. Phys. Chem. Lett. 3 (2012) 1727–1731.
[37] M.J. Bleda-Martínez, J.A. Maciá-Agulló, D. Lozano-Castelló, E. Morallón, D. Cazorla-Amorós, A. Linares-Solano, Role of surface chemistry on electric double layer capacitance of carbon materials, Carbon 43 (2005) 2677–2684.
[38] C. Vix-Guterl, E. Frackowiak, K. Jurewicz, M. Friebe, J. Parmentier, F. Béguin, Electrochemical energy storage in ordered porous carbon materials, Carbon 43 (2005) 1293–1302.
[39] E. Raymundo-Piñero, K. Kierzek, J. Machnikowski, F. Béguin, Relationship between the nanoporous texture of activated carbons and their capacitance properties in different electrolytes, Carbon 44 (2006) 2498–2507.
[40] S. Kumagai, D. Tashima, Electrochemical performance of activated carbons prepared from rice husk in different types of non-aqueous electrolytes, Biomass Bioenerg. 83 (2015) 216–223.
[41] P. Bonhote, A. Dias, N. Papageorgiou, K. Kalyanasundaram, M. Gratzel, Hydrophobic, highly conductive ambient-temperature molten salts, Inorg. Chem. 35 (1996) 1168–1178.
[42] R.S. Kühnel, N. Boeckenfeld, S. Passerini, M. Winter, A. Balducci, Mixtures of ionic liquid and organic carbonate as electrolyte with improved safety and performance for rechargeable lithium batteries, Electrochim. Acta 56 (2011) 4092–4099.
[43] A.B. Fuertes, M. Sevilla, High-surface area carbons from renewable sources with a bimodal micro-mesoporosity for high-performance ionic liquid-based supercapacitors, Carbon 94 (2015) 41–52.
[44] A. Balducci, R. Dugas, P.L. Taberna, P. Simon, D. Plee, M. Mastragostino, S. Passerini, High temperature carbon-carbon supercapacitor using ionic liquid as electrolyte, J.Power Sources 165 (2007) 922–927.
[45] T. Tooming, T. Thomberg, H. Kurig, A. Jaenes, E. Lust, High power density supercapacitors based on the carbon dioxide activated D-glucose derived carbon electrodes and 1-ethyl-3-methylimidazolium tetrafluoroborate ionic liquid, J.Power Sources 280 (2015) 667–677.
[46] A. Balducci, U. Bardi, S. Caporali, M. Mastragostino, F. Soavi, Ionic liquids for hybrid supercapacitors, Electrochem. Commun. 6 (2004) 566–570.
[47] G. Ayalneh Tiruye, D. Muñoz-Torrero, J. Palma, M. Anderson, R. Marcilla, All-solid state supercapacitors operating at 3.5 V by using ionic liquid based polymer electrolytes, J.Power Sources 279 (2015) 472–480.
[48] D. Cericola, R. Koetz, A. Wokaun, Effect of electrode mass ratio on aging of activated carbon based supercapacitors utilizing organic electrolytes, J.Power Sources 196 (2011) 3114–3118.
[49] V. Khomenko, E. Raymundo-Pinero, F. Beguin, A new type of high energy asymmetric capacitor with nanoporous carbon electrodes in aqueous electrolyte, J.Power Sources 195 (2010) 4234–4241.
[50] A. Orita, K. Kamijima, M. Yoshida, Allyl-functionalized ionic liquids as electrolytes for electric double-layer capacitors, J.Power Sources 195 (2010) 7471–7479.